Analysis of Microstructural Characteristic Changes in Carbonate Rocks Due to Mechanical Deformation: A Comparative Pre- and Post-Mortem Study Based on X-Ray Micro-CT Imaging

PPMI PENELITIAN FMIPA ITB (Fakultas/KK) 2026, Skema: Hibah Penelitian Kompetitif

Fourier Dzar Eljabbar Latief [1], Alvina Kusumadewi Kuncoro[1], Umar Fauzi[1], Muhammad Rizqie Arbie[1]

[1] KK Fisika Bumi dan Sistem Kompleks, Fakultas Matematika dan Ilmu Pengetahuan Alam, Institut Teknologi Bandung

Abstract

Carbonate reservoirs exhibit high microstructural heterogeneity, complicating geomechanical predictions for hydrocarbon recovery and carbon capture, utilization, and storage (CCUS). This study investigates mechanical deformation-induced microstructural changes in carbonate rocks by integrating uniaxial compressive strength (UCS) testing with 3D X-ray micro-computed tomography (micro-CT) under a comparative pre- and post-mortem scheme. Multiscale scanning (0.69–20 μm) reveals hidden pore complexity, with porosity increasing from <0.1% at the macroscale to 15%–58% at the microscale. Mechanical testing of two siliclastic carbonate samples shows that pre-existing fractures and laminae govern failure: fractured sample T1 undergoes brittle axial splitting at 4.51 GPa peak stress (12.11 GPa Young's modulus), whereas intact sample T2 forms compaction bands, reaching 11.23 GPa (11.69 GPa modulus) before diagonal fracturing. Post-mortem 3D analysis demonstrates total porosity increases from 1.21% to 4.02% (T1) and 1.12% to 2.80% (T2), alongside increased connectivity density (9.56 to 25.43 mm⁻³ in T1), quantitatively linking intrinsic pore architecture to macroscopic rock strength for subsurface storage modeling.

Keywords: Carbonate rocks; X-ray micro-CT; Mechanical deformation; Uniaxial compression test; Digital rock physics

Introduction

Carbonate formations serve as vital reservoirs for hydrocarbon recovery and geological carbon capture, utilization, and storage (CCUS). However, their pronounced microstructural heterogeneity and complex pore networks make geomechanical behavior difficult to predict using conventional macroscopic testing alone. While standard uniaxial compressive strength (UCS) tests quantify bulk elastic and failure parameters, surface-level visual inspections cannot capture internal micro-fracture evolution prior to catastrophic failure. X-ray micro-computed tomography (micro-CT) overcomes this limitation by enabling non-destructive, three-dimensional visualization and phase segmentation of mineral matrices and pore spaces across multiple resolution scales. Implementing a comparative pre- and post-mortem micro-CT imaging scheme provides a rigorous framework for evaluating deformation-induced structural damage. Pre-test (pre-mortem) scans establish baseline 3D pore geometry, connectivity, and pre-existing weak planes, whereas post-test (post-mortem) imaging maps fracture propagation pathways, crack coalescence, and matrix fragmentation. Quantitative 3D morphometric comparison between pre- and post-failure volumes—evaluating porosity, specific surface area, Euler number, connectivity density, and fractal dimension—further characterizes internal damage evolution. Integrating pre- and post-loading micro-CT analysis with uniaxial compression testing thus links intrinsic pore architecture to macroscopic rock strength, supporting wellbore stability and subsurface storage integrity.

Research Method

To evaluate deformation-induced microstructural evolution, this study integrates uniaxial compressive strength (UCS) testing with comparative pre- and post-mortem X-ray micro-computed tomography (micro-CT) imaging. From a large siliclastic carbonate core-Slab sample, cylindrical core plugs cP alongside multiscale subsamples were imaged on a SkyScan 1173 and 2214 down to 0.69 μm. Additional core-Plug samples (T1 and T2) of 2 cm in diameter were initially scanned in their intact pre-mortem state using a Bruker SkyScan 1173 at 130 kV, 61 mA, and a 20.0 μm pixel size. Reconstructed 3D volumes established baseline pore architecture and pre-existing weak planes for sample T2 in particular.

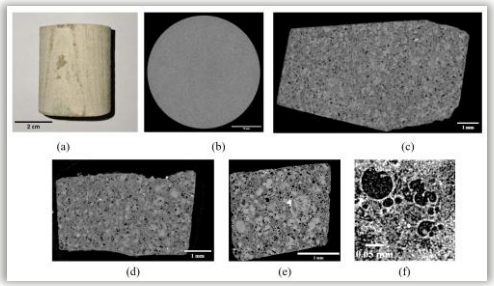

Figure 1. *(a) Core-plug sample; and μ-CT images: (b) cP [20 μm/pix], (c) mP5 [5 μm/pix], (d) mP9 [5.71 μm/pix], (e) μP1 [1 μm/pix], and (f) μP2 [0.69 μm/pix].*

Subsequently, samples T1 and T2 underwent displacement-controlled UCS loading using an Instron 5985 testing system until macroscopic failure. Recorded stress-strain curves were analyzed to quantify peak stress, proportional limit, 0.2% offset yield strength, resilience modulus, and Young's modulus, determined from the purely linear elastic region. Immediately after failure, fractured specimens underwent post-mortem micro-CT scanning under identical tomographic acquisition parameters. Quantitative 3D morphometric analysis was conducted in CTAn on pre- and post-test volumes (total, open, and closed porosity, specific surface area, crack aperture, Euler number, connectivity density, and fractal dimension). Finally, structural alterations and Kachanov's damage factor were correlated with mechanical parameters and macroscopic fracture orientations to link intrinsic microstructure with rock strength.

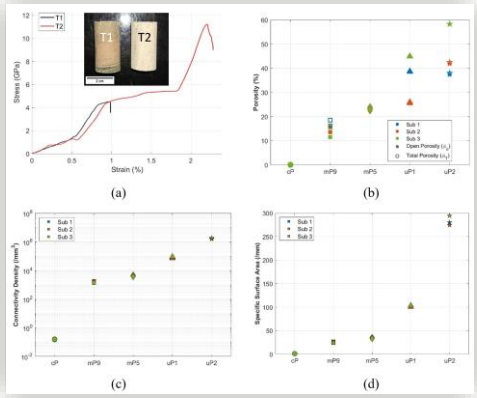

Figure 2. *(a) Core-plug T1 and T2 and the stress-strain curves of T1 and T2; and microstructural parameters for various sample sizes: (b) porosity, (c) connectivity density, and (d) specific surface area.*

Results & Discussions

Multiscale micro-CT imaging (**Fig. 1** and **Fig. 2b–d**) shows strong resolution dependency in characterizing carbonate pore architecture. Macro-scale scans (cP, 20 μm) under-estimate total porosity ($< 0.1\%$), sub-micron imaging (mP9 to μP2, 5.71–0.69 μm) resolves interconnected pore throats, porosities of 15%–58%, connectivity densities (C_d) up to $\sim 10^6$ mm^{-3}, and specific surface areas (S_v) ~300 mm^{-1}. Under uniaxial com-pression (**Fig. 2a**), both core plugs exhibit com-parable linear elastic moduli (12.11 GPa for T1; 11.69 GPafor T2) but divergent failure regimes. Sample T1 failed at 4.51 GPa, whereas intact T2 develops a strain-hardening compaction band before failing at 11.23 GPa. Comparative pre- and post-mortem tomography (**Fig. 3**) links this mechanical contrast to fracture evolution. In T1 (**Fig. 3a–d**), pre-existing laminae act as weak planes guiding axial splitting, increasing total porosity (ϕ_t) from 1.21% to 4.02%, open porosity from 1.05% to 3.65%, S_v from 0.77 to 1.59 mm^{-1}, and C_d from 9.56 to 25.43 mm^{-3}. T2 (**Fig. 3e–h**) experiences pore collapse prior to diagonal shear-extensional fracturing, raising $\phi_t$from 1.12% to 2.80% and S_v from 1.71 to 3.92 mm^{-1}. Evaluating Kachanov's damage factor confirms that microstructural damage is governed by initial fabric. Sample T1 records a 68.6% higher dama-ge factor ($D = 0.0285$) than T2 ($D = 0.0169$) because lamina-guided axial splitting maximizes net void generation ($\Delta\phi_t = +2.81\%$). In T2, compaction-induced pore closure partially offsets fracture dilation ($\Delta\phi_t = +1.68\%$), resulting in lower bulk damage while preserving matrix integrity ($D < 0.03$).

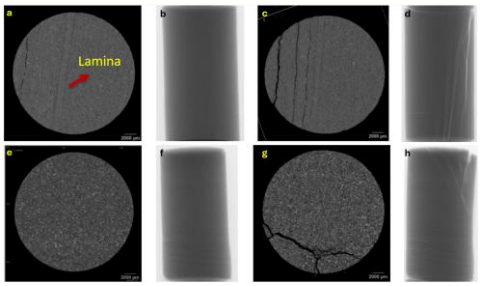

Figure 3. *Micro-CT image of T1 pre-test (a) cross section (b) longitudinal section, post-test (c) cross section (d) longitudinal section, and T2 sample pre-test (e) cross section (f) longitudinal section, post-test (g) cross section (h) longitudinal section.*

Conclusion

Multiscale X-ray micro-CT reveals intricate, interconnected pore networks hidden at coarser macroscales. Integrating pre- and post-mortem imaging with uniaxial compression testing demonstrates that initial microstructural fabric governs failure mechanisms: pre-existing laminae induce brittle axial splitting, whereas intact matrices undergo ductile compaction before diagonal fracturing, linking intrinsic pore architecture to macroscopic rock strength.

Acknoledgement

The authors thank ITB for funding this research through PPMI 2026 (Competitive Scheme) program number FMIPA.PPMI-1-51-2026.